NUCL SCI TECH (2018) 29:107
https://doi.org/10.1007/s41365-018-0450-9

Real-time wide-range neutron flux monitor for thorium-based molten salt reactor

Xiang Zhou[1,2] · Zi-Hao Liu[1,2] · Chao Chen[1,2] · Guo-Qing Huang[3] · Ze-Jie Yin[1,2]

Received: 15 August 2017 / Revised: 28 February 2018 / Accepted: 20 March 2018 / Published online: 3 July 2018

Abstract A novel full-digital real-time neutron flux monitor (NFM) has been developed for thorium-based molten salt reactor (TMSR). The system is based on the high-speed, parallel, and pipeline processing of the field programmable gate array as well as the high-stability controller area network platform. A measurement range of 10^8 counts per second is achieved with a single fission chamber by utilizing the normalization of the count and Campbell algorithms. With the advantages of using the measurement range, system integrity, and real-time performance, digital NFM has been tested in the Xi'an pulsed reactor fission experiments and was found to exhibit superior experimental performance.

Keywords Neutron flux monitor · Real time · Thorium-based molten salt reactor · Campbell

This work was supported by the National Natural Science Foundation of China (Nos. 11375195 and 11575184) and the National Magnetic Confinement Fusion Energy Development Research (No. 2013GB104003).

✉ Zi-Hao Liu
lzhh1234@mail.ustc.edu.cn

1 State Key Laboratory of Particle Detection and Electronics, University of Science and Technology of China, Hefei 230026, China

2 Department of Modern Physics, University of Science and Technology of China, Hefei 230026, China

3 Shanghai Institute of Applied Physics, Shanghai 201800, China

1 Introduction

The molten salt reactor (MSR) is one possible type of future fourth-generation reactor, and the thorium MSR (TMSR) program, which is a pilot research project of the Chinese Academy of Sciences for the next 10 years, aims to establish a 2-MW TMSR by 2020 [1–4]. As the fission intensity in the reactor directly correlates with the neutron flux, it is essential to monitor the fluctuation of the latter in the core region. Moreover, as a means to guarantee safety during the long-term operation of the reactor, such a monitoring could provide early warning before accidents occur. Thus, the design of the neutron flux monitor (NFM) [5, 6] system, including the detector and electronic system, is important for the TMSR.

Four of the most common methods for neutron measurement include nuclear recoil, nuclear reaction, nuclear activation, and nuclear fission. Furthermore, the most common detectors that employ the nuclear recoil method [7] include the hydrogen proportional counter (HPC), semiconductor recoil counter (SRC), and organic scintillator (OS). The HPC is mainly applied to the 0.01–1.5 MeV energy region because of the limitation of the recoil proton range. However, in order to obtain an accurate neutron flux, SRC requires the energy spectrum of the recoil proton and a modification through the Monte Carlo method. On the other hand, OS is highly sensitive to gamma rays, which could produce pulse signals with a similar amplitude to neutrons, making it difficult to distinguish the neutron signal. The typical nuclear reaction detectors that are commonly applied for neutrons with less than 1 MeV of energy are BF_3 and ^3He proportional counters [8]. This is particularly significant because of the presence of low-energy neutrons, which have considerably larger reaction cross sections compared with high-energy neutrons in these detectors. The self-powered detector (SPD) is based on nuclear activation methods [9] and has been applied for NFM in the reactor core. However, the results of SPD cannot be obtained in real time. Another common detector in the field of neutron detection is the fission chamber (FC), which was previously applied to the Shin-Wolsong Nuclear Power Generating Stations designed by Thermo Fisher Scientific [10]. Based on the nuclear fission method [11, 12], FC features a wide measurement range and superior real-time performance with an excellent gamma suppression ability, making it ideal for our design of TMSR–NFM.

As for the design of the electronic system for NFM, analog comparators are commonly applied as key components in this circuit design. However, comparator-based analog circuits are often difficult to maintain or modify [13]. Moreover, because the reactor always has a considerably wide neutron flux range, a combination of multiple FCs with different sensitivities is frequently applied. This requires different sets of electronic systems, making the system overly complex. For this case, we developed a fully digitized NFM that is able to obtain real-time information on the neutron flux in the reactor with a single FC. The NFM is based on the application of the field programmable gate array (FPGA) [14] and controller area network (CAN) platform. After a 250-MHz analog-to-digital (ADC) sampling, FPGA is able to collect and process the sampled neutron waveforms in real time using both parallel and pipeline architecture. Two NFM algorithms, the count and Campbell algorithms, are both implemented in FPGA and can be automatically switched according to the practical experimental scenario, extremely extending the measurement range of the system. The NFM has been applied in the Xi'an pulsed reactor (XAPR), and experimental results are presented in this paper.

The rest of the article proceeds as follows. Section 2 presents a detailed design of the NFM system, including system structure, electronic system, and FPGA algorithms. In Sect. 3, the experimental performance of NFM is provided, and discussion and conclusions are presented in Sect. 4.

2 Design

2.1 Hardware

In the design of the NFM system, we aim to improve its measurement range and real-time performance while reducing the scale of the system. The specific requirements are as follows:

(a) Wide measurement range.
(b) Superior real-time performance.
(c) High system integrity.

In order to increase the measurement range, two different discrimination algorithms are also applied and combined as one in real-time calculation. The real-time performance of the system is achieved by utilizing the parallel processing of massive data by FPGA. Additionally, the application of FC as the detector, along with the fully digitized electronic discrimination system, greatly improves the integrity of the system.

Figure 1 depicts the system structure of the TMSR–NFM system. It mainly consists of two parts: detection and discrimination.

2.1.1 Detection

As shown in Fig. 1, the detection function consists of ^{235}U FC, as well as the preamplifier. Because of the wide range and low uncertainty of the reaction cross section, ^{235}U FC has no limitations on the energy of the incident particle, making it applicable to the incident neutron with primary energy varying from 0 to 200 MeV. The fission reactions between neutrons and ^{235}U in FC generate two fission fragments with kinetic energy between 40 and 110 MeV. The fragments are multiply charged heavy ions and considerably easy to ionize, generating strong current pulses in ^{235}U FC. This is accomplished by calculating the amount of fragments the flux of the input neutron can obtain. Because current pulses induced by fission fragments are considerably stronger than the current induced by the γ-ray, ^{235}U FC provides great advantages on background γ suppression.

To minimize the noise induced by the cable between the preamplifier and FC and to improve the output signal-to-noise ratio, the broadband current preamplifier is applied. Moreover, in order to allow the output voltage of a single neutron signal to range between 0.5 and 1 V, the total amplification factor of the preamplifier is set according to the quantity of electric charge induced by a single neutron in FC.

2.1.2 Discrimination

Figure 2 indicates the structure of the discrimination function, including the signal processing unit (SPU) and host system.

An essential part of the TMSR–NFM system is SPU, which processes the input signal to obtain real-time neutron counts. The output signal of the preamplifier is connected to SPU through a long cable. The analog signal processing circuit first adjusts the input amplitude and then converts

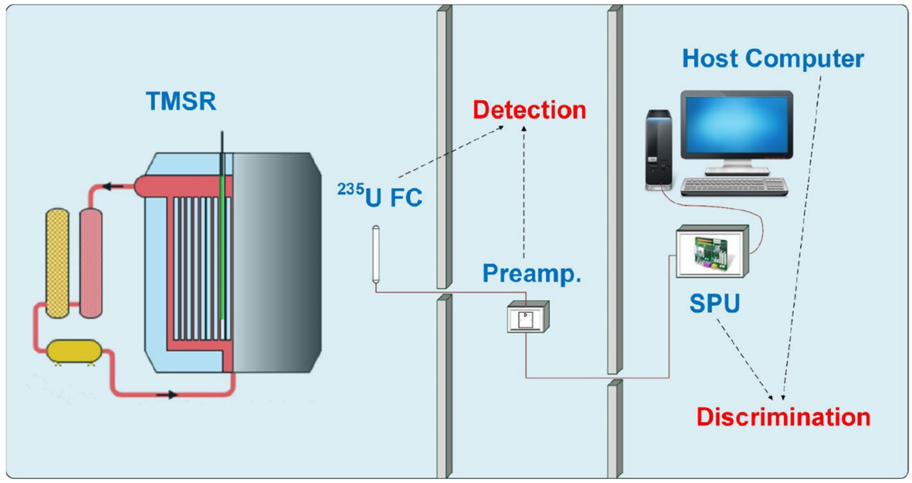

Fig. 1 (Color online) Structure of TMSR–NFM

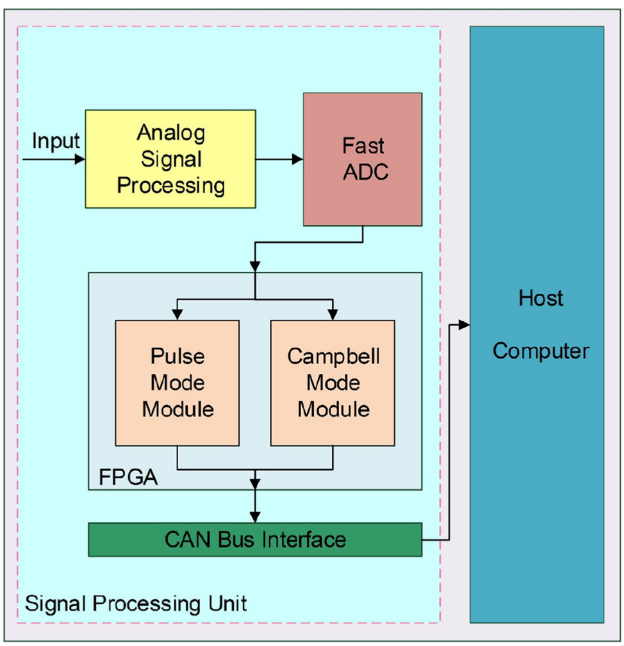

Fig. 2 (Color online) SPU structure

the single-ended signal into differential ones in order to satisfy the requirement of the 250-MHz, 12-bit ADC. Thereafter, the digitized data stream is directly transferred to FPGA for further data processing.

The NFM algorithms and flow control are all realized in FPGA. In this process, Altera Cyclone III EP3C16Q240C8 [15] is applied in SPU to perform the following functions.

(a) Calculate the input baseline offset. In the self-checking mode, the input baseline offset is calculated and recorded, and then deducted from the ADC measurement as a means to obtain actual input signals during the NFM operation.
(b) The implementation of the count and Campbell algorithms is realized. Both algorithms operate in parallel, and results are simultaneously uploaded to the host.
(c) Multiple functions for the interaction between the host and SPU, including the SPU self-check, trigger processing, data upload, and realization of CAN protocol, as well as system instructions and settings, were implemented.

The communication between the host and SPU is via the CAN bus, which is mainly used for system settings and upload of neutron signals from FC. The application of the CAN bus guarantees the quality of data communication by taking advantage of its superior real-time performance, long transmission range, and high electromagnetic immunity.

2.2 Algorithm

When FPGA receives digitized data stream from ADC, the primary objective is to precisely determine the number of neutron signal pulses. When the neutron flux is sufficiently low to the extent that individual neutron pulses barely have overlaps, the pulses can be counted using the count algorithm. Additionally, when the flux is high, the Campbell algorithm can be used to obtain a result that is proportional to the actual neutron flux. Moreover, in the design of TMSR–NFM, both algorithms were applied for different neutron flux scenarios, and we managed to unite the results into one intact waveform as a means to broaden the flux measurement range.

2.2.1 Count algorithm

When the neutron flux is relatively low, neutron pulses are discrete, and their amplitudes are considerably stronger than other signals are. Thus, by setting a proper noise threshold and discriminating the pulses with amplitudes beyond that threshold, an accurate number of neutron pulses can be obtained. This simple method remains available when the input neutron count is lower than 4×10^5 counts per second (cps). However, when the input flux exceeds the given value, miss counting would occur because pulses pile up, and the bias would increase when the flux intensifies.

2.2.2 Campbell algorithm

Under a high neutron flux situation, we applied the Campbell algorithm to obtain the neutron pulse count from the output neutron waveform of FC. The Campbell theory states that the output of a nuclear detector is subjected to the Poisson distribution through time. Furthermore, when it undergoes a linear time-invariant system with an impulse response of $h(t)$, the variance of the output voltage at time t is as follows:

$$\sigma^2(v) = \lambda \overline{Q^2} \int_0^\infty h^2(t)\mathrm{d}t, \tag{1}$$

where v is the output voltage at time t, Q is the current impact strength, $h(t)$ is the impulse response of a linear time-invariant system, and λ is the average output pulse number of the detector.

For the same fission reactor and detector, $\bar{Q}^2$ is a constant, whereas for the same preamplifier, $\int_0^\infty h^2(t)\mathrm{d}t$ is a constant. From Eq. (1), the variance of the continuous output voltage is proportional to the neutron flux; thus, the neutron pulse number can be calculated. The Campbell algorithm is employed when the neutron count is greater than 4×10^4 cps. When the flux is lower, irrelevant signals and noises gain larger proportions in the input signal, potentially affecting the accuracy of the algorithm.

2.2.3 Normalization

Figure 3 depicts the result of a simulation test of the algorithms. Simulated neutron pulses are generated by Keysight 81160A Pulse Function Generator, and the neutron pulse numbers individually calculated by the two algorithms are plotted as ordinates. In the figure, yellow dots represent the calculation result of the count algorithm, whereas blue dots represent that of the Campbell algorithm. The figure also shows that the available measuring range of the count algorithm is between 0 and 4×10^5 cps, whereas that of the Campbell algorithm is between 4×10^4 and 10^8 cps. An overlap between the two regions exists, where both algorithms can work properly, so that the results of the two algorithms should be linear, as follows:

$$y_{\text{count}} = a x_{\text{Campbell}} + b. \tag{2}$$

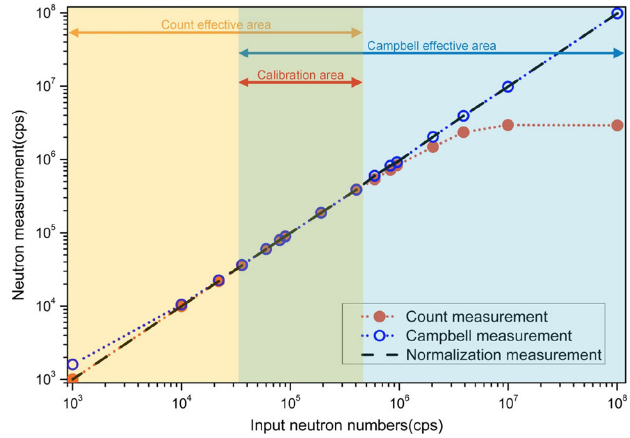

Fig. 3 (Color online) Simulation test results of count and Campbell algorithms

Utilizing linear fitting on Eq. (2), the values of a and b can be obtained so that all calculated Campbell results can be converted to an actual count value. The count waveform can be obtained by unitizing results from the two algorithms and intact neutron. The count algorithm results are applied when the flux is below 10^5 cps, and the Campbell algorithm results are applied when the flux is above 10^5 cps. The combination of the two methods made it possible to overcome the respective limitations of each algorithm on the applicable neutron flux range, which considerably broadens the total measurement range of the system.

3 Performance

3.1 Experiments

In the performance test, Keysight 81160A Pulse Function Generator is used to generate simulated neutron pulse signals [16] with an amplitude of 250 mV, a pulse width of 200 ns, and consistency with the Poisson distribution. Moreover, a 150-mV noise signal is added on the pulse signals, as shown in Fig. 4a.

By changing the expected value of λ, of the Poisson distribution, different numbers of neutrons were generated. Sixteen cases with neutron numbers of 10^3, 2×10^4, 4×10^4, 6×10^4, 8×10^4, 10^5, 2×10^5, 4×10^5, 6×10^5, 8×10^5, 10^6, 2×10^6, 4×10^6, 6×10^6, 10^7, and 10^8 were generated. Figure 4b shows the scenario of 10^5 cps neutrons with a150-mV noise overlapped.

Simulation signals are transmitted into SPU through a twisted pair cable. Figure 5 demonstrates the SPU count errors in those cases by comparing the measurement and expected values of neutron counts. Results have shown that during such cases, the maximum error of SPU is lower than

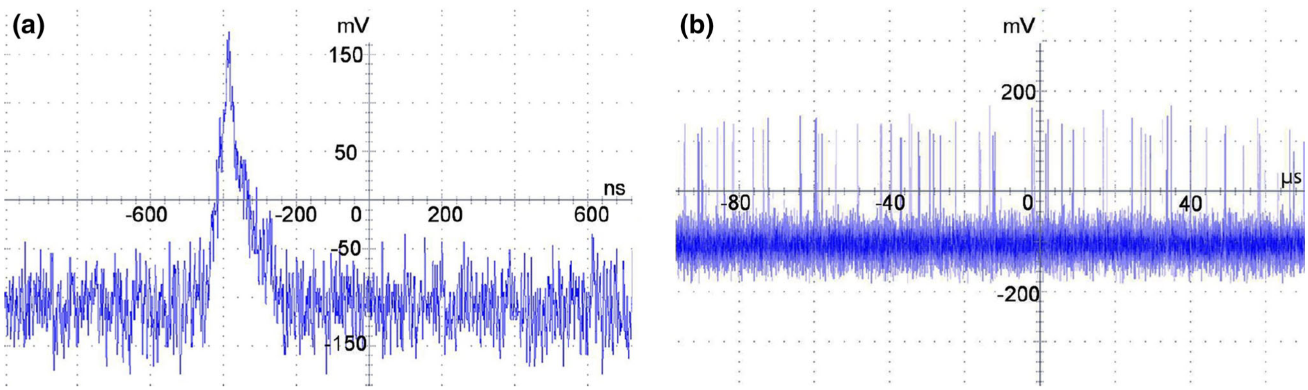

Fig. 4 (Color online) Simulated neutron pulses. **a** A simulated neutron pulse signal with noise overlapped and **b** the scenario of 10^5 cps neutrons with noise overlapped

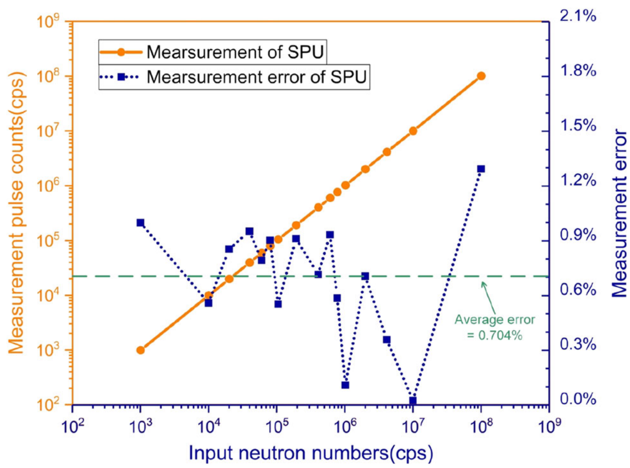

Fig. 5 (Color online) Experiments by imitated neutron pulse

1.5% and the average error is lower than 0.8%; these indicate that SPU exhibits considerable neutron measurement ability under different neutron flux conditions.

3.2 Application experiments

The Xi'an pulsed reactor [17–19] is the first multi-functional pulse reactor with a steady-state rated power of 2 MW and maximum pulse peak power of 4200 MW designed and built in China. It is composed of the reactor, supply system, and experimental irradiation facility. It has six control rods, and the intensity of the reaction is controlled by the insertion and extraction of these rods. A photograph of XPAR is shown in Fig. 6. As indicated in the figure, FC was placed inside the device through the iron gate.

In the experiment, we utilized an LB124 ^{235}U FC from the China National Nuclear Corporation. It is cylindrical with an external diameter of 50 mm and a length of 546 mm. Its shell is covered with titanium. The sensitive volume is 354 mm long, and the sensitivity of the hot

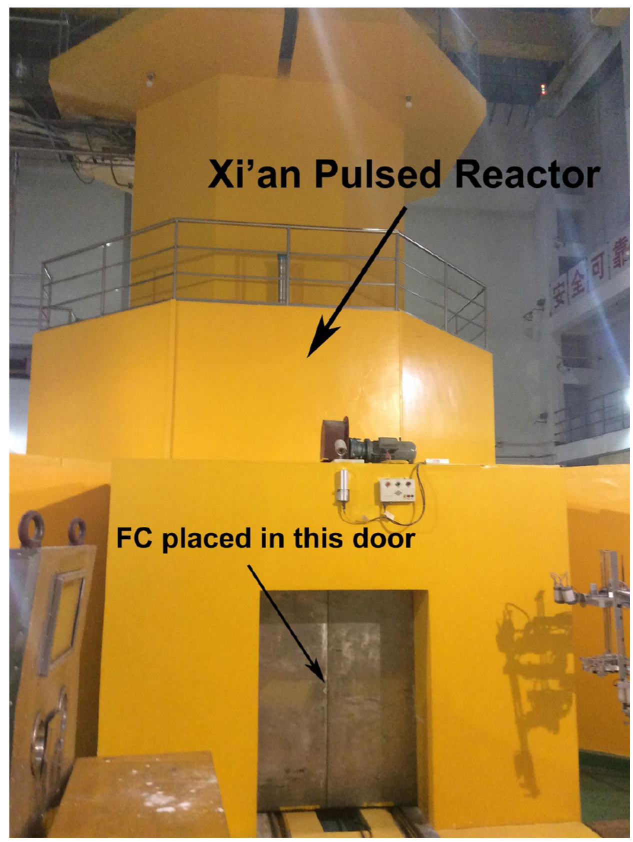

Fig. 6 (Color online) Photograph of the Xi'an pulsed reactor

neutron is approximately 0.8 cps/(n cm^{-2} s^{-1}). A 15-m triaxle cable connects FC and the preamplifier, providing a − 702-V working voltage to FC. The output of the preamplifier is then transmitted to SPU through a 20-m-long twisted pair cable for further processing.

3.2.1 *Reactor background*

When all the control rods were dropped, and the reactor was not operating, we conducted the neutron background count test, which lasted for 14.283 h. The neutron count value was obtained every second, and a total of 51,418 measurement results are plotted in Fig. 7, revealing the fluctuation of the background neutron counts of the reactor. The experiment demonstrates the appreciable real-time performance and stability of the NFM system.

3.2.2 Reactor operation

As shown in Fig. 8, for the first 143 s, all control rods remained in full insertion. From 144 to 882 s, the control rods were extracted at certain speeds, and the neutron flux increased. A total time of 341 s was measured for the sampled neutron counts, which increased from 5×10^3 to 5×10^7 cps. At 754 s, the sampled neutron count reached the upper limit of the system of 1.08×10^8 cps. Because of the output scale of the preamplifier, the output voltage of the preamplifier reached its upper limit. This limited the measurement range of SPU when the neutron count from FC exceeds 1.08×10^8 cps. However, a slight waveform drop could be observed. Because the input signal exceeds the measurement range of the preamplifier at that time, the transistor quiescent operation point would shift, and the output gain of the preamplifier would decrease because of the transistor's operating characteristics. From 882 to 1488 s, the control rods were inserted, and 343 s elapsed for the neutron count to decrease from 5×10^7 to 5×10^3 cps. From 1488 to 1517 s, the control rods remained still. From 1517 to 2170 s, the rods were extracted for a second time. The time that elapsed for the neutron count to increase from 5×10^3 to 5×10^7 cps was 348 s. The time spent during each period was approximately equal, because the insertion and extraction of the control rods had the same velocity.

Because the insertion and extraction speeds of the control rods were fixed, the neutron flux in the reactor developed exponentially [20, 21]. As shown in Fig. 9, sampled neutron counts during the extraction of the second control rod were exponentially fitted. From 1566 to 1941 s, the sampled neutron count increased from 2×10^3 to 5×10^7 cps, during which the measurement value fitted well with the exponential function model (R^2 = 0.9897).

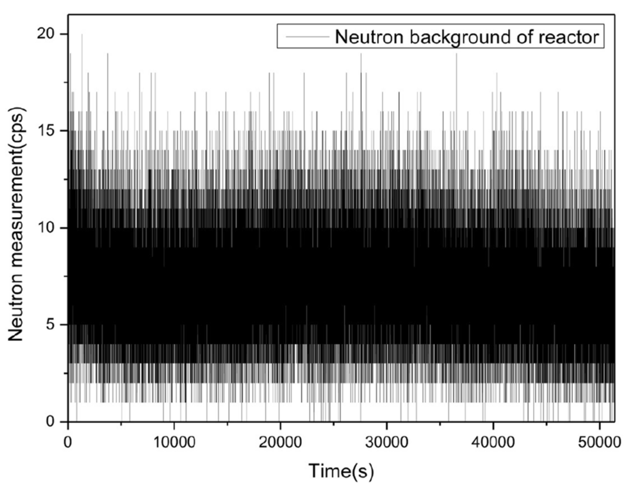

Fig. 7 The measurement of reactor background

4 Discussion and conclusions

A novel NFM system based on FPGA and CAN bus has been designed for TMSR. A wide measuring range, up to 10^8 cps [22], is achieved with a single FC by utilizing the combination of both the count and Campbell algorithms programmed in FPGA. The real-time neutron count results are uploaded to the host through the CAN bus. A simulation test, using simulated neutron signals, has effectively proven the performance of the NFM system. Experimental results at TMSR have also been presented, which prove the stability and accuracy of the system when used over

Fig. 8 (Color online) Measurements during reactor operation

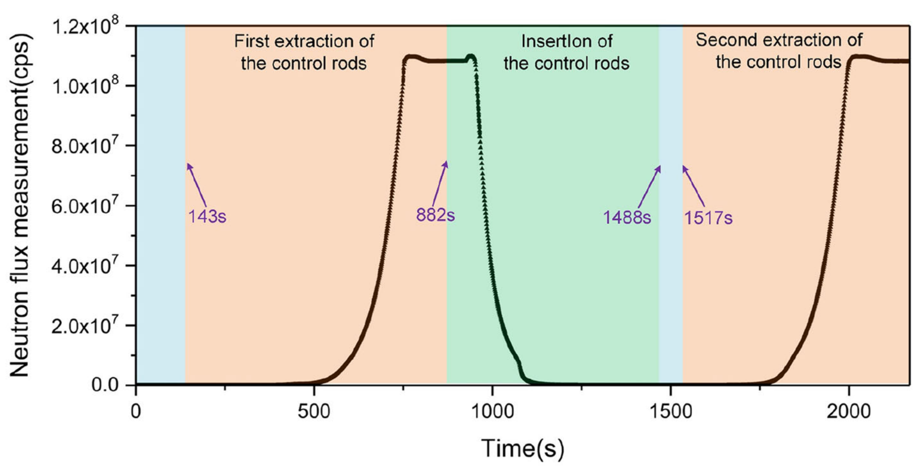

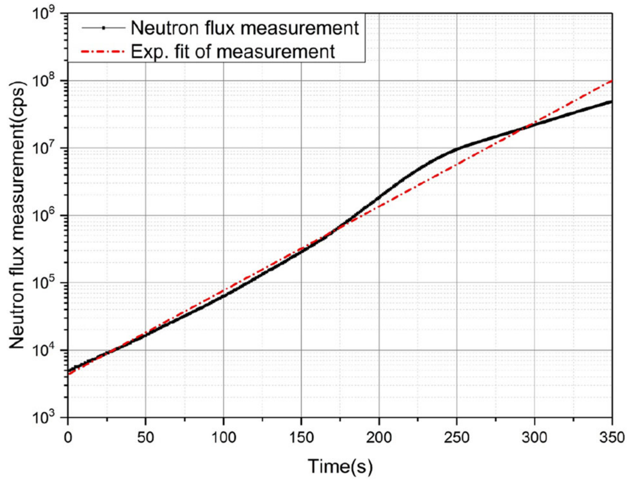

Fig. 9 (Color online) Exponential fit during the extraction of control rods

extended periods of field operations. The NFM system aims at replacing the traditional analog nuclear measurement instruments in the future.

Work is ongoing to design a new preamplifier with an adjustable gain, which can be controlled by FPGA. By decreasing the gain of the amplifier when the flux is high, the upper limit of the preamplifier measuring range is increased so that the NFM measuring range could be broadened. This design is expected to improve the measuring range of NFM by up to 10^{10} cps.

References

1. R.M. Ji, M.H. Li, Y. Zou et al., Impact of photoneutrons on reactivity measurements for TMSR-SF1. Nucl. Sci. Technol. **28**, 76 (2017). https://doi.org/10.1007/s41365-017-0234-7
2. J. Yin, Y. Ma, Y. Qian et al., Experimental investigation of the bubble separation route for an axial gas–liquid separator for TMSR. Ann. Nucl. Eng. **97**, 1–6 (2016). https://doi.org/10.1016/j.anucene.2016.06.018
3. L.F. Han, Y.Z. Chen, J. Cai et al., The application of EPICS in TMSR radiation protection and access control system. Nucl. Sci. Technol. **27**, 41 (2016). https://doi.org/10.1007/s41365-016-0040-7
4. C.C. Yin, N. Zhang, Y.P. Li et al., The design of RMT-based IOC redundancy at RCPI experimental platform in TMSR. Nucl. Sci. Technol. **25**, 060402 (2014). https://doi.org/10.13538/j.1001-8042/nst.25.060402
5. S.A. Wender, S. Balestrini, A. Brown et al., A fission ionization detector for neutron flux measurements at a spallation source. Nucl. Instrum. Methods A **336**, 226–231 (1993). https://doi.org/10.1016/0168-9002(93)91102-S
6. J.W. Yang, Q.W. Yang, G.S. Xiao et al., Fusion neutron flux monitor for ITER. Plasma Sci. Technol. **10**, 141 (2008). https://doi.org/10.1088/1009-0630/10/2/01
7. N.P. Hawkes, N.J. Roberts, Digital dual-parameter data acquisition for SP2 hydrogen-filled proportional counters. Radiat. Prot. Dosim. **161**, 253–256 (2013). https://doi.org/10.1093/rpd/nct262
8. S. Pszona, A. Bantsar, P. Tulik et al., Low-level gamma and neutron monitoring based on use of proportional counter filled with 3He in polythene moderator: study of the responses to gamma and neutrons. Radiat. Prot. Dosim. **161**, 237–240 (2013). https://doi.org/10.1093/rpd/nct274
9. A. Taheri, A. Pazirandeh, Measurements of the thermal neutron flux for an accelerator-based photoneutron source. Australas. Phys. Eng. Sci. Med. **39**, 857–862 (2016). https://doi.org/10.1007/s13246-016-0477-3
10. A. Shirley, EMC testing of Korean next generation reactors nuclear instrumentation systems. Trans. Am. Nucl. Soc. **101**, 311–312 (2009)
11. R. Liu, T.H. Zhu et al., Reaction rates in blanket assemblies of a fusion–fission hybrid reactor. Nucl. Sci. Technol. **23**, 242 (2012). https://doi.org/10.13538/j.1001-8042/nst.23.242-246
12. S.P. Li, X.F. Xu, H.R. Cao et al., Dynamic linear calibration method for a wide range neutron flux monitor system in ITER. Nucl. Sci. Technol. **24**, 040402 (2013). https://doi.org/10.13538/j.1001-8042/nst.2013.04.002
13. A.K. Mishra, S.R. Shimjith, T.U. Bhatt et al., Kalman filter-based dynamic compensator for vanadium self powered neutron detectors. IEEE Trans. Nucl. Sci. **61**, 1360–1368 (2014). https://doi.org/10.1109/TNS.2014.2321340
14. Y. Xu, X. Ji, Q. Yang et al., Development of a low-drift integrator system on the HL-2A tokamak. Rev. Sci. Instrum. **87**, 023507 (2016). https://doi.org/10.1063/1.4940027
15. C. Chen, W.W. Fan, Y.H. Pan et al., A multi-channel real-time digital integrator for magnetic diagnostics in HL-2A tokamak. Nucl. Sci. Technol. **27**, 14 (2016). https://doi.org/10.1007/s41365-016-0006-9
16. C. Yuan, Y.P. Li, Y.F. Huang, Simulation study on digital processing of fission chamber output signal. Nucl. Technol. **38**, 010401 (2015). https://doi.org/10.11889/j.0253-3219.2015.hjs.38.010401. **(in Chinese)**
17. L.P. Wang, X.P. Jiang et al., Calculation and experimental validation of ~ (127) I transmutation rate in Xi'an pulsed reactor. Nucl. Power Eng. **25**, 233–236 (2014). https://doi.org/10.3788/hplpb20132501.0233. **(in Chinese)**
18. D. Li, W.S. Zhang, X.B. Jiang, Parameter measurement for radiation field of large space neutron irradiation platform in Xi'an pulsed reactor. At. Energy Sci. Technol. **48**, 1243–1249 (2014). https://doi.org/10.7538/yzk.2014.48.07.1243. **(in Chinese)**
19. B. Rajesh, N. Kariya, M. Ichikawa, Dehydrogenation of cyclohexane over Ni based catalysts supported on activated carbon using spray-pulsed reactor and enhancement in activity by addition of a small amount of Pt. Catal. Lett. **105**, 83–87 (2005). https://doi.org/10.1007/s10562-005-8009-x
20. Z.M. Sergei, Methods, methodologies and formulas for simplified neutronics analyses of fusion reactors. J. Nucl. Sci. Technol. **31**, 867–878 (1994). https://doi.org/10.3327/jnst.31.867
21. H.K. Joo, C.H. Kim et al., A new approach to core-reflector boundary conditions for nodal reactor computations. Nucl. Sci. Eng. **116**, 300–312 (1994). https://doi.org/10.13182/NSE94-A18989
22. R.L. Fleischer, P.B. Price, R.M. Walker, Neutron flux measurement by fission tracks in solids. Nucl. Sci. Eng. **22**, 153–156 (1965). https://doi.org/10.13182/NSE65-A20234